EUROPEAN FUSION DEVELOPMENT AGREEMENT

EFDA–JET–PR(01)72

M J Mantsinen et al

Analysis of Ion Cyclotron Heating and Current Drive at $\omega \approx 2\omega_{cH}$ for Sawtooth Control in JET Plasmas

Analysis of Ion Cyclotron Heating and Current Drive at $\omega \approx 2\omega_{cH}$ for Sawtooth Control in JET Plasmas

M.J.Mantsinen[1], C.ngioni[2], L.-G.Eriksson[3], A.Gondhalekar[4], T.Hellsten[5,6], T.Johnson[6], M.-L.Mayoral[4,3], K.G.McClements[4], M.F.F.Nave[7], F.Nguyen[3], S.Podda[8], J.Rapp[9], O.Sauter[2], S.E.Sharapov[4], E.Westerhof[10]
and contributors to the EFDA-JET workprogramme

[1]Helsinki University of Technology, Association Euratom-Tekes, Finland
[2]CRPP, Association EURATOM-Confédération Suisse, EPFL, Lausanne, Switzerland
[3]Association EUR TOM/CEA,CEA Cadarache, Saint-Paul-Lez-Durance, France
[4]Euratom/UKAEA Fusion Association, Culham Science Centre, Abingdon, Oxon, OX14 3DB, United Kingdom
[5]EFDA Close Support Unit, Culham, United Kingdom
[6]Alfvén Laboratory, Association Euratom-VR, Stockholm,Sweden
[7]Associação EUR TOM-IST, Centro de Fusão Nuclear,Lisboa,Portugal
[8]Associazione EUR TOM-ENEA sulla Fusione, Frascati, Rome, Italy
[9]Institut für Plasmaphysik, Forschungszentrum Jülich GmbH, EURATOM Association, TEC, Jülich, Germany
[10]FOM-Rijnhuizen, Association Euratom-FOM, TEC, Nieuwegein, The Netherlands

Analysis of ion cyclotron heating and current drive at $\omega \approx 2\omega_{cH}$ for sawtooth control in JET plasmas*

M.J. Mantsinen[1], C. Angioni[2], L.-G. Eriksson[3], A. Gondhalekar[4], T. Hellsten[5,6], T. Johnson[6], M.-L. Mayoral[4,3], K.G. McClements[4], M.F.F. Nave[7], F. Nguyen[3], S. Podda[8], J. Rapp[9], O. Sauter[2], S.E. Sharapov[4], E. Westerhof[10] and contributors to the EFDA-JET workprogramme+

[1]Helsinki University of Technology, Association Euratom-Tekes, Finland
[2]CRPP, Association EURATOM-Confédération Suisse, EPFL, Lausanne, Switzerland
[3]Association EURATOM/CEA, CEA Cadarache, Saint-Paul-Lez-Durance, France
[4]Euratom/UKAEA Fusion Association, Culham Science Centre, Abingdon, Oxon, OX14 3DB, United Kingdom
[5]EFDA Close Support Unit, Culham, United Kingdom
[6]Alfvén Laboratory, Association Euratom-VR, Stockholm, Sweden
[7]Associação EURATOM-IST, Centro de Fusão Nuclear, Lisboa, Portugal
[8]Associazione EURATOM-ENEA sulla Fusione, Frascati, Rome, Italy
[9]Institut für Plasmaphysik, Forschungszentrum Jülich GmbH, EURATOM Association, TEC, Jülich, Germany
[10]FOM-Rijnhuizen, Association Euratom-FOM, TEC, Nieuwegein, The Netherlands

Abstract Ion cyclotron heating and current drive at $\omega \approx 2\omega_{cH}$ in JET deuterium plasmas with a hydrogen concentration $n_H/(n_D+n_H)$ in the range of 5-15% are analysed. Second-harmonic hydrogen damping is found to be maximised by placing the resonance on the low-field-side (LFS) of the torus, which minimises competing direct electron damping and parasitic high-harmonic D damping in the presence of D beams. The shape of the calculated current perturbation and the radial localisation of the heating power density for the LFS resonance are consistent with the experimentally observed evolution of the sawtooth period when the resonance layer moves near the q=1 surface. Since the calculated driven current is dominated by a current of diamagnetic type caused by finite orbit widths of trapped resonating ions, it is not too sensitive to the ICRF phasing. Control of sawteeth with ion cyclotron current drive using the LFS $\omega \approx 2\omega_{cH}$ resonance in the present experimental conditions can thus be best obtained by varying the resonance location rather than the ICRF phasing. Due to differences in fast ion orbits, collisional electron heating and fast ion pressure profiles are significantly more peaked for a LFS resonance than for a high-field-side (HFS) resonance. For the HFS $\omega \approx 2\omega_{cH}$ resonance, an enhanced neutron rate is observed in the presence of D beam ions, which is consistent with parasitic D damping at the $\omega \approx 5\omega_{cD}$ resonance in the plasma centre.

---

* This article is an extended version of a contribution to the 28th EPS Conference on Controlled Fusion and Plasma Physics held at Funchal, Madeira, Portugal, June 2001.

+ See appendix of J. Paméla, *et al*., "Overview of Recent JET Results and Future Perspectives," Fusion Energy 2000 (Proc. 18th Int. Conf. Sorrento, 2000), IAEA, Vienna (2001).

1. Introduction

Non-inductive control of the plasma current profile plays an important role in achieving improved plasma confinement and stability properties in tokamak plasmas. For example, localised modifications of the plasma current profile are required for sawtooth control, stabilisation of neoclassical tearing modes (NTMs) and tailoring of the current profile in the advanced modes of operation. Ion cyclotron current drive (ICCD) is one of the non-inductive current drive methods which has been used to modify the current profile locally in tokamak plasmas. On JET the sawtooth period has been varied in ICRF-only discharges by more than one order of magnitude due to changes in the magnetic shear $s = (r/q)(\mathrm{d}q/\mathrm{d}r)$ near q = 1, using hydrogen minority ($\omega \approx \omega_{\mathrm{cH}}$) ICCD [1, 2]. Here, $q \approx rB_{\mathrm{T}}/(RB_{\mathrm{p}})$ is the tokamak safety factor, r and R are the minor and major radii, respectively, and B_{T} and B_{p} are the toroidal and poloidal component of the magnetic field, respectively. More recently, experiments have been carried out on JET with ICRF waves tuned to the second harmonic hydrogen resonance ($\omega \approx 2\omega_{\mathrm{cH}}$) to affect the sawtooth period and amplitude in discharges with ICRF only and in discharges with combined ICRF and NBI [3-5]. The aim of these experiments was to control the m = 3, n = 2 NTM seed island by controlling the sawtooth behaviour [3-5]. Here, m and n are the poloidal and toroidal mode numbers, respectively. In this article, ion cyclotron heating and current drive in these experiments are analysed in detail.

The method of driving current by heating either minority ions with toroidally directed waves at a frequency equal to the ion cyclotron frequency, or majority ions at harmonics of the cyclotron frequency, was originally proposed by Fisch [6]. The Fisch current drive mechanism can briefly be described as follows. Owing to the Doppler shift of the cyclotron resonance, $\omega - n\omega_{\mathrm{ci}} - k_{\|}\mathrm{v}_{\|} = 0$, directed waves interact resonantly with either co-going or counter-going ions, depending on which side of the cyclotron resonance the interaction takes place and on the direction of the wave propagation. For example, consider passing ions on the low field side of the resonance and $k_{\|} > 0$. In this case the wave interacts only with ions having a positive parallel velocity, i.e. $\mathrm{v}_{\|} > 0$. As a result of the wave-particle interaction, ions with $\mathrm{v}_{\|} > 0$ are accelerated mainly in the perpendicular direction. This creates an anisotropic ion distribution function. In particular, there will be a depletion of ions with $\mathrm{v}_{\|} > 0$ in the bulk of

the distribution, whereas there will be an enhancement of ions at higher energies. Collisional pitch-angle scattering will try to restore an isotropic distribution. However, the strength of the pitch-angle scattering is strongly velocity dependent, decreasing as $1/v^3$. Therefore, it will smooth out the distribution function more effectively at low energies than at high energies. Consequently, there will be an effective transfer of ions from the region with $v_{\|} < 0$ to the region $v_{\|} > 0$, and thus a driven current. For waves propagating in the same toroidal direction as the plasma current, the Fisch mechanism predicts a positive (negative) fast ion current with respect to the plasma current for flux surfaces having $\omega > n\omega_{ci}$ ($\omega < n\omega_{ci}$) as they intersect the mid-plane on the same side of the magnetic axis as the unshifted resonance $\omega = n\omega_{ci}$.

The Fisch model for ICCD does not take into account acceleration of ions by waves in the parallel velocity, finite orbit widths of the resonating ions, or trapped ions. When these effects are included, new mechanisms to drive current appear [7, 8]. For example, the finite orbit widths of trapped resonating ions give rise to a current of diamagnetic type (analogous to the seed of the neoclassical bootstrap current) [7], while in the thin banana width approximation used in the Fisch model it is only the passing ions that contribute to the driven current. The current density profile generated by trapped ions is always bipolar and modifies the plasma current gradient around the resonance surface. When ICRF power per particle is high or the resonance is on the low field side of the torus, ICRF-accelerated ions tend to be mainly trapped and the contribution to the driven current by trapped resonating ions becomes the dominating one [7, 8]. Indeed, in such cases the total fast ion current can even be in the opposite direction than that given by the Fisch model, as pointed out in Refs [7, 8].

While several experimental and theoretical studies have been performed to investigate ICCD and sawtooth activity with $\omega \approx \omega_{cH}$ (see e.g. Refs 1, 2 and 7-9), previous knowledge on using second harmonic ICRF schemes is sparse. Sawtooth control with $\omega \approx 2\omega_{cH}$ in 50%:50% hydrogen-deuterium plasmas on JET has been reported earlier [1], but many issues concerning second harmonic ICCD remain unexplored. For example, at the second harmonic of the ion cyclotron frequency ICRF waves tend to interact with a small number of ions with relatively high energy, typically in excess of the critical energy [10] for equal ion and electron power partition. As the Fisch model predicts the ICCD efficiency to be maximum for fast ions with energies of the order of the critical energy, it is not obvious whether significant ICCD can be

obtained with a second harmonic scheme. Also, the dependence on the concentration of the heated species has not been addressed experimentally. Owing to the tendency of second harmonic ICRF schemes to preferentially create very energetic ions, second harmonic ICCD could be suited for studies of the new current drive mechanisms discussed in Refs 7 and 8. Studies of ICCD with second harmonic schemes also have a reactor relevant aspect owing to the $\omega \approx 2\omega_{cT}$ scheme foreseen as the main ICRF scenario to be used in deuterium-tritium plasmas in next-step reactors.

In the experiments analysed in this article, ICRF waves were tuned to the $\omega \approx 2\omega_{cH}$ resonance either on the high (HFS) or low field side (LFS) using either waves propagating predominantly in the co-current or counter-current direction (+90° or –90° phasing, respectively) to provide localised ICCD. The ICRF frequency was 42 MHz, ICRF power up to 4.5-5 MW and the hydrogen concentration $n_H/(n_D+n_H)$ was varied in the range of 5-15%. The effect on the sawtooth period was demonstrated in ICRF-only discharges with a ramp in the magnetic field and plasma current to change the resonance location at constant q. Subsequently, discharges with combined ICRF and NBI heating were performed with a ramp in NBI power at a constant magnetic field and plasma current. From the ICRF physics point of view, the added NBI power can lead to new effects as the NBI injected deuterons are also resonant with the ICRF waves.

In order to assess whether ICCD with $\omega \approx 2\omega_{cH}$ can affect sawteeth in the present experiments, we have used the ICRF codes PION [11,12] and FIDO [13] in order to analyse and quantify the different ICRF-related quantities. The PION code, which calculates the time-evolution of the velocity distribution functions of the resonating ions and the ICRF power deposition self-consistently, has been used to gain insight into the overall ICRF power partitioning and performance in these discharges. Using the prescribed wave field consistent with the PION code results, the three-dimensional Monte Carlo code FIDO has been utilised for detailed modelling of the resonating ion distribution and the ion cyclotron current drive. In this modelling finite-orbit-width effects and ICRF-induced transport of fast ions, giving rise to the new current drive mechanisms as discussed in Refs 7 and 8, are taken into account. The PRETOR transport code [14] with a sawtooth trigger model outlined in Section 2 (and first introduced in Ref. 15) has been used to assess whether the calculated ICRF current drive and local heating power density are large enough to affect the sawtooth stability in the discharges.

The outline of this article is as follows. After a discussion on sawtooth stability and the different ICRF effects that can play a role for sawteeth in Section 2, the ICRF modelling tools PION and FIDO are described briefly in Section 3. The results from the simulations are presented in Section 4. Finally, the results are summarised and discussed in Section 5.

2. Sawtooth stability

Sawtooth oscillations are periodic relaxations of the plasma core parameters that are caused by an internal kink mode with toroidal n = 1 and dominant poloidal m = 1 mode numbers. While they can be beneficial, for example for the removal of plasma impurities, there are several drawbacks associated with them. These include limiting the core plasma pressure and triggering neoclassical tearing modes and other instabilities.

It is well established that in addition to affecting sawteeth via modifications to the magnetic shear near q = 1 through localised current drive, ICRF heating can also have a stabilising effect on sawteeth by building up fast ion pressure inside the q = 1 surface [16-18]. The stabilising effect comes from ICRF-heated ions having bounce-averaged precessional drift frequencies $\omega_{\mathrm{D,fast}}$ in excess of the mode frequency ω [19]. In this case, the trapped ion orbits complete many toroidal revolutions during the time scale of the variation of the mode, so that the magnetic fluxes through the toroidal trajectories of the centres of these orbits are adiabatically conserved (third adiabatic invariant). This can prevent the growth of the mode. The localised (electron) heating by ICRF waves can also play a role for sawtooth stability by affecting the magnetic shear, s, and (electron) pressure gradient, as has been assessed with experiments with electron cyclotron resonance heating on TCV [20-22].

The relative importance of the different physical mechanisms on sawtooth stability can be quantified by considering the following threshold conditions for triggering sawtooth crashes:

$$-\delta\hat{W}_{\mathrm{core}} / \tau_{\mathrm{A}} > c_{\mathrm{h}} \omega_{\mathrm{D,fast}} \quad (1)$$

$$-\delta\hat{W} / \tau_{\mathrm{A}} > \omega_{*\mathrm{i}} / 2 \quad (2)$$

$$-c_{\hat{\rho}}\hat{\rho}/\tau_{\mathrm{A}} < -\delta\hat{W}/\tau_{\mathrm{A}} < \omega_{*\mathrm{i}}/2 \quad \text{and} \quad s_{\mathrm{crit}} < s_1 \qquad \text{(3a) and (3b)}$$

These conditions have been invoked in order to predict the period of sawtooth oscillations in ITER and are applicable provided that the auxiliary condition $\omega_{\mathrm{D,fast}} > \omega_{*\mathrm{i}}$ is satisfied [15]. According to this model, a sawtooth crash is triggered if any of the above three criteria is satisfied. Here, the dimensionless n = 1, m = 1 internal kink mode energy functional $\delta\hat{W} = \delta\hat{W}_{\mathrm{core}} + \delta\hat{W}_{\mathrm{fast}}$ is defined so that in the ideal MHD limit the mode growth rate is given by $\gamma = -\delta\hat{W}/\tau_{\mathrm{A}}$, where $\delta\hat{W}_{\mathrm{core}}$ and $\delta\hat{W}_{\mathrm{fast}}$ are contributions from the core plasma and fast particles, respectively, $\tau_{\mathrm{A}} = \sqrt{3}R_0/c_{\mathrm{A}}$, c_{A} is the Alfvén speed and R_0 is the major radius. Furthermore, c_{h} and $c_{\hat{\rho}}$ are constants of order unity, $\omega_{*\mathrm{i}}$ is the ion diamagnetic frequency at q = 1, $\hat{\rho} = \sqrt{\rho_{\mathrm{i}}^2 + \rho_{\mathrm{s}}^2}/r_1$, ρ_{i} is the thermal ion Larmor radius, $\rho_{\mathrm{s}}^2 = \rho_{\mathrm{i}}^2 T_{\mathrm{e}}/T_{\mathrm{i}}$, and r_1 is the q = 1 radius.

When the first sawtooth trigger criterion given by Eq. (1) is satisfied, the internal kink mode growth rate $-\delta\hat{W}_{\mathrm{core}}/\tau_{\mathrm{A}}$ is too fast for the high-energy ions to have a sufficient stabilising influence. When the second criterion given by Eq. (2) is satisfied, $-\delta\hat{W}/\tau_{\mathrm{A}}$ overcomes the stabilisation due to thermal ion diamagnetic effects. When the third criterion given by Eq. (3a) is satisfied, layer physics around the q = 1 surface plays a crucial role. In this case the reconnecting mode becomes unstable when the growth rate exceeds a finite value determined by electron and ion diamagnetic effects [23]. This criterion can be written in the form of Eq. (3b) where the critical shear s_{crit} at q = 1, proportional to the local profile gradients, is given by different expressions depending on whether the mode is destabilised in the resistive or ion-kinetic regimes. In both cases, there is a strong dependence on various parameters evaluated at q = 1 [15].

3. ICRF modelling tools used

In order to quantify the different ICRF-related quantities that can play a role for sawteeth in the present experiments, the ICRF codes PION [11, 12] and FIDO [13] have been used. In this section the main features of the codes that are important for the present analysis are discussed.

3.1 The PION code

The PION code [11, 12] calculates the time evolution of the ICRF power deposition profiles using a model (i.e. superposition of two components, one in the limit of strong absorption and one in the limit of weak absorption) [24, 25] that closely reproduces the results from the full wave code LION [26]. The output of the power deposition calculation is used to calculate the time evolution of the one-dimensional pitch-angle-averaged velocity distribution function(s) of the resonating ions. In the calculation of the ICRF power deposition, the effects of the pitch-angle-averaged distribution functions of the resonating ions, including those of injected beam ions that are resonant with ICRF waves [27], are taken into account. Self-consistent calculation of the power deposition and the distribution functions is especially important for high-harmonic heating schemes such as the $\omega \approx 2\omega_{cH}$ scheme considered in this article. The reason for this is that high-harmonic damping, which is normally rather weak for a thermal plasma, is significantly enhanced when a tail of energetic ions starts to develop in the ion distribution function as a result of interaction with the ICRF wave. The usual assumption of the classical slowing down and confinement of fast ions is made and the finite-orbit-width effects are taken into account in a simplified way by assuming that the fast ions are trapped and that they have turning points close to the cyclotron resonance. The collision coefficients used in the calculation of the pitch-angle-averaged ion distribution functions are then averaged over the resulting orbits.

For the magnetic fields and ICRF frequency used in the present experiments, not only $\omega \approx 2\omega_{cH} = 4\omega_{cD}$ but also $\omega \approx 3\omega_{cD}$, $\omega \approx 5\omega_{cD}$ and $\omega \approx 3\omega_{cH} = 6\omega_{cD}$ can reside in the plasma, depending on the chosen magnetic field (cf. Fig. 1). With the implemented version of the power deposition model [24, 25] in PION, only one resonance layer location for a given ICRF frequency can be taken into account. In the simulations presented in this article, we have considered the $\omega \approx 2\omega_{cH} = 4\omega_{cD}$ resonance since it has been found to give rise to the largest single pass damping. The effect of the $\omega \approx 5\omega_{cD}$ resonance has been considered separately at the lowest magnetic fields (i.e. when this resonance is located in the plasma centre between the low field side ICRF antennas and the $\omega \approx 2\omega_{cH}$ resonance, cf. Fig. 1). Here, the main aim has been to investigate whether damping at this resonance could be responsible for the enhanced fusion reactivity observed at these magnetic fields in the presence of deuterium beam ions.

All the input data used in the PION simulations presented in this article are taken directly from the JET experimental database. The hydrogen concentration was deduced from the D_α and H_α emission at the plasma edge, and was assumed to be spatially constant.

3.2 The FIDO code

For detailed modelling of the ICRF-driven hydrogen ion distribution function and the current driven by these ions, we have used the three-dimensional FIDO code [13]. The FIDO code solves the three-dimensional orbit-averaged Fokker-Planck equation [28]

$$\frac{\partial f_0}{\partial t} = \langle C(f_0) \rangle + \langle Q(f_0) \rangle$$

with a Monte-Carlo method, taking into account the effects of the RF-induced radial transport of fast ions [29] and finite orbit widths. Here, the distribution function f_0 is a function of three invariants of the unperturbed particle motion, <...> denotes averaging over unperturbed orbits, C is the collision operator describing collisions with background ions and electrons and Q is the quasi-linear operator describing the wave-particle interaction.

In the FIDO simulations presented in this article, input data such as density and temperature profiles have been taken directly from the JET experimental database for required time points during the discharges. The hydrogen power deposition and wave parameters, such as the perpendicular wave number and the polarisation, are adjusted to be consistent with those given by the PION code. Thus, the ion distribution functions are calculated for prescribed power deposition profiles given by PION. Since the effects of RF-induced transport, which can modify the power deposition by modifying the ion distribution functions [30], are not significant in the present experiments according to FIDO modelling, this procedure is fairly reasonable. In order to keep the total ICRF power absorbed by protons constant in the FIDO simulations, the magnitude of the electric field is adjusted after each time step. During tests of the code it has been verified that the collisional power transfer to the background plasma equals the input power in the steady state. In the FIDO simulations discussed in this article, the proton distribution function is assumed to be Maxwellian with a temperature equal to the background ion temperature at the beginning of the simulations, and the proton distribution function is evolved until a steady state is reached.

4. Results

The aim of the experiments analysed in this article was to investigate the role of the sawteeth on the onset of the $m = 3$, $n = 2$ neoclassical tearing modes (NTMs) [3-5]. NTMs are routinely triggered in NBI-only discharges on JET only at relatively low magnetic fields, i.e. below 1.7 T [3-5]. Consequently, the experiments analysed in this article (c.f. Table 1) were carried out at magnetic fields in the range of 1.2-1.6 T. ICRF power was applied both with and without NBI in order to modify sawteeth with localised ion cyclotron current drive [3-5]. The NBI power was up to 17 MW. The operational frequencies of the JET ICRF antennas and the required magnetic field range led to the choice of the second harmonic hydrogen scenario. Up to 4.5-5 MW of ICRF power was used at an ICRF frequency of 42 MHz, placing the $\omega \approx 2\omega_{cH}$ resonance either on the high (HFS) or low field side (LFS) depending on the magnetic field. The approximate locations of the different hydrogen and deuterium ion cyclotron resonance layers are shown in Fig. 1 as a function of the toroidal magnetic field. Both +90° and –90° phasings were used to launch the ICRF waves predominantly in the co-current and counter-current direction, respectively.

In the following, results from the analysis of ICRF heating and current drive in the discharges summarised in Table 1 are presented. First, ICRF-only discharges are considered in Section 4.1, followed by discharges with combined NBI and ICRF in Section 4.2.

4.1. ICRF-only discharges

4.1.1 $\omega \approx 2\omega_{cH}$ resonance on the low field side with –90° phasing

The possibility of affecting the sawtooth period with ICRF waves was studied in ICRF-only discharges using ramps in the magnetic field B and the plasma current to change the resonance location with respect to the inversion radius, q and ICRF power being held constant. With the $\omega \approx 2\omega_{cH}$ resonance on the LFS (discharge 51800 with –90° phasing, cf. Table 1), minima in the sawtooth period were observed as the resonance moved through the inversion radius in time (Fig. 2). It is difficult to explain such behaviour in terms of sawtooth stabilisation by the fast ion pressure alone [19], since for a fixed ICRF power as in the present discharge this is expected to give rise to more stabilisation the further the resonance is inside the q=1 surface.

According to PION, about 95% of the ICRF power is absorbed by H and the rest by direct electron damping via electron Landau damping (ELD) and transit time magnetic pumping (TTMP) (Fig. 3). The calculated tail temperature of the fast protons is about 5-10 times the critical energy E_{crit} [10] of about 20 keV ($T_e \approx 2$ keV) at which protons transfer energy equally to background electrons and ions. Consequently, mainly collisional electron heating is obtained as shown in Fig. 4. The presence of fast protons is confirmed indirectly by observations of Alfvén eigenmodes (AEs) driven by fast ions. The magnetic fluctuation spectrograms, as measured with the magnetic pick up coils [31,32] at the plasma edge, are shown in Fig 5a. Both toroidal and elliptical Alfvén eigenmodes (TAEs and EAEs) in the frequency ranges of 100-140 kHz and 240-300 kHz, respectively, are seen in the measured spectrum. The observation of AEs is a good indicator of the presence of fast ions with velocities comparable to Alfvén velocity in the plasma. In the present plasma conditions, fast protons with energies above 100 keV have velocities exceeding the Alfvén velocity.

The current density driven by ICRF-accelerated protons together with collisional electron heating profile and fast proton energy density, as given by the FIDO code, are shown in Fig. 6. The calculated current perturbation j_{fast} decreases the magnetic shear in a narrow (≈10 cm) region just outside the resonance layer and increases the shear on both sides of this narrow region. The calculated current is dominated by the current of diamagnetic type [7], caused by the large orbit widths of the resonating trapped high-energy protons. Note that this current is in the opposite direction as compared with the fast ion driven current due to passing ions taken into account in the Fisch model [6], which predicts an increase in the shear around the resonance and decrease in the shear further away from the resonance. The maxima of $|j_{fast}|$ as shown in Fig. 6 are displaced with respect to the maxima in the fast ion pressure and collisional electron heating profiles which coincide roughly with the radial location of the reversal of the driven current. The net contribution to the local current density, after correcting for the back current carried by electrons [33-36], is about 3-6%. In the simulations shown in Fig. 6, a hydrogen concentration η_H of about 12.5% has been used (cf. Table 1). We have also assessed the sensitivity of j_{fast} to η_H assumed in the simulations. As η_H is varied between 5–20%, $|j_{fast}|$ increases somewhat (≈10-25%) with η_H, while the radial shape of j_{fast} stays roughly the same. The current drive via ELD and TTMP has been assessed separately with the LION code [26] and has been found negligible as compared with the fast ion driven current.

Unfortunately, no good-quality motional Stark effect data on the current profile exist for comparisons with simulations for this discharge or other discharges analysed in this article due to poor signal-to-noise ratio at low magnetic fields.

4.1.2 $\omega \approx 2\omega_{cH}$ resonance on the low field side with +90° phasing

In Fig. 6 results from FIDO modelling are also shown for a discharge prepared in the same way as discharge 51800 with -90° phasing described above but with +90° phasing of ICRF antennas (discharge 51801, cf. Table 1). As we can see, not only the fast proton energy density and collisional electron heating profiles, but also the current driven by ICRF-heated protons have similar shapes and magnitudes to those with -90° phasing. The reason for this is that in both cases the current is dominated by a contribution of diamagnetic type [7], caused by the finite orbit widths of the resonating trapped protons. The presence of similar populations of fast protons is supported by measurements of AE mode activity driven by fast ions in the two discharges (cf. Figs 5a and 5b). The sawtooth behaviour is also similar [4].

4.1.3 $\omega \approx 2\omega_{cH}$ resonance on the high field side with –90° phasing

In order to establish a regime where the driven current is consistent with the Fisch model for ion cyclotron current drive by passing ions, experiments have been carried out with the $\omega \approx 2\omega_{cH}$ resonance on the HFS. Moving the resonance from the LFS to the HFS increases the number of passing since in the HFS resonance case the ICRF-accelerated ions are closer to the boundary between trapped and passing orbits.

With the resonance on HFS (discharge 51796 with –90° phasing, cf. Table 1), direct electron damping increases according to PION code simulations as compared with a LFS resonance (Figs 3 and 7). The fast ion driven current given by FIDO (cf. Fig. 6a) is such that it decreases the magnetic shear around the ICRF resonance. Indeed, the FIDO simulations show that in this discharge the contribution from the passing ions to the driven current dominates, and the current profile modification is in the same direction to that expected from the Fisch model [6]. Furthermore, as shown in Figs. 6b and 6b, the calculated collisional electron heating and fast ion pressure profiles for a HFS resonance are significantly broader than for a LFS resonance. These differences are due to the different characters of the orbits of the resonating ions for

LFS and HFS resonances. We illustrate these differences in Figs 8a and 8b, where we have considered representative samples of Monte Carlo particles as given by the FIDO code simulations in an orbit classification diagram outlined in Ref. 37. In this diagram the invariants of the unperturbed fast particle motion are normalised as $\hat{\lambda} = \lambda R / \delta_{\mathrm{p}}$ and $\hat{P}_{\varphi} = [2q_0 / (B\delta_{\mathrm{p}}^2)]P_{\varphi} / Ze$, where λ is defined by $\lambda = E / (\mu B_0) - 1$, $\delta_{\mathrm{p}} = (2q_0\rho / R)^{2/3} R$ is the characteristic orbit width, ρ is the Larmor radius and $P_{\varphi} = mR\mathrm{v}_{\varphi} + Ze\psi$ is the toroidal angular momentum (ψ is the poloidal flux). The different regions of this diagram are discussed extensively in Ref. 37.

As can be seen in Fig. 8b for discharge 51800 with a LFS resonance, the non-thermal resonating ions occupy mainly the standard trapped region VII. For discharge 51796 with a HFS resonance, orbits in the standard trapped region VII decreases and orbits in regions I-VI, corresponding to a significant number of passing ions, increases as can be seen in Fig. 8a.

Differences in the ICRF-driven fast ion population in discharge 51796 as compared with discharges 51800 and 51801 are supported by differences in the observed AEs characteristics (cf. Fig. 5). In particular, the amplitude of EAEs is lower and the amplitude of TAEs is higher for discharges 51800 and 51801 with LFS resonance. Since the eigenfunction of the TAE has a ballooning structure, while the eigenfunction of the EAE has anti-ballooning components [38], these results are consistent with a presence of a stronger population of fast ion orbits on the HFS in discharge 51796. The presence of fast protons with energies well above the critical energy [10] in discharge 51796 is also confirmed by high-energy neutral-particle analyser (NPA) measurements [39] (for discharges discussed in Sections 4.1.1 and 4.1.2 NPA data are not available).

4.1.4. Analysis of sawtooth stability with the PRETOR code

We will next investigate, using the PRETOR transport code [14] with the sawtooth trigger model outlined in Section 2, whether the calculated ICCD and local heating power density are large enough to affect the sawtooth stability in the present discharges. In this investigation we have concentrated in discharge 51800 (cf. Section 4.1.1) since more relevant experimental data are available for this discharge than other discharges considered in this article. The

PRETOR analysis will be followed at the end of this Section by the assessment of the fast ion effects through the fast ion contribution $\delta\hat{W}_{\text{fast}}$ to the $n = 1$, $m = 1$ internal kink mode energy.

In the PRETOR simulations the calculated ICCD profile given by FIDO for discharge 51800 (c.f. Fig. 6a) was taken into account using a fit consisting of two components: one counter-current drive component and one co-current drive component. The radial profiles of both components, together with the radial profile of the electron heating power density, were assumed to be Gaussians with profile widths fitting the FIDO results. For simplicity, the radial profile shapes were kept fixed while the radial locations of the maxima of the counter current drive density, the heating power density and the co current drive density were assumed to follow the time evolution of the resonance position. The resulting time-evolutions are shown in Fig. 9b together with the simulated $q = 1$ radius. According to FIDO simulations carried out for different resonance locations in this discharge (c.f. also Fig. 12 for a comparison between two different pulses with different resonance locations), these simplifications should be fairly reasonable and reproduce the right theoretical trend. The main difference between the profiles used in the PRETOR simulations and those given by FIDO for different resonance locations concerns the magnitudes of the driven current and the profile widths. While in PRETOR simulations the profile shapes and thus the amplitudes of the current and heating power densities are kept fixed, the FIDO simulation shows that $|j_{\text{fast}}|$ and the widths of the current and electron heating power density profiles decrease by about 40% when the resonance moves from r/a ≈ 0.3 to 0.6. In the PRETOR simulations the Rebut-Lallia-Watkins transport [40] coefficients have been adjusted so that the simulated temperature profiles match the experimental temperature profiles, while the density profile has been kept fixed, given by a smoothed time-averaged experimental density profile. However, the resulting qualitative picture of the sawtooth period behaviour does not critically depend on the choice of the specific transport model.

PRETOR code simulations (excluding fast particle effects on the $n = 1$, $m = 1$ internal kink mode energy functional $\delta\hat{W}$, i.e. assuming $\delta\hat{W}_{\text{fast}} = 0$) show that the driven current and electron heating in Fig. 6 are large and localised enough to affect the sawteeth in the present experimental conditions. In particular, the PRETOR results indicate that the calculated current perturbation and electron heating profiles are broadly consistent with the observed time

behaviour of the sawtooth period when the resonance location moves in time (cf. Figs 2 and 9). Both current drive (co and counter) components and the heating power density are important for the shear in the sawtooth trigger criterion in Eq. (3b). Co-current drive close to q = 1, and heating power localisation close to and outside q = 1, have a stabilising effect on sawteeth since they slow down the build-up of the shear after a sawtooth crash. Counter-current drive close to q = 1, and heating power localisation close to and inside q = 1, have the opposite, destabilising effect on sawteeth since they enhance the build-up of the shear after a sawtooth crash. The experimentally observed sequence of two maxima and minima between t = 23.7-25.5 s in the sawtooth period in Fig. 2 is then ascribed to the shifts among (the maxima of) the current drive components and (the maximum of) the heating power density. Indeed, when the different components of the driven current (counter, co or both) or the heating power density are excluded in the PRETOR simulations, the time evolution of the sawtooth period is different from that shown in Fig. 9. The observed effects of the current drive and heating power localisation are consistent with experimental observations with electron cyclotron resonance heating on TCV [20-22]. A more detailed account on the PRETOR analysis of these discharges will be presented in a separate paper.

In order to quantify fast ion effects on sawteeth through the fast ion contribution $\delta\hat{W}_{\mathrm{fast}}$ to the n = 1, m = 1 internal kink mode energy, we have used the procedure outlined in the Appendix to calculate $\delta\hat{W}_{\mathrm{fast}}$. At the time of the local minimum in the sawtooth period in Fig. 2, $t \approx$ 25.3 s, we obtain $\delta\hat{W}_{\mathrm{fast}} \approx -5\times10^{-3}$ from Eq. (A.2) using parameters consistent with the present modelling and measured data. In comparison, both $\delta\hat{W}_{\mathrm{core}}$ and $\hat{\rho}$ at this time are of the order of 3×10^{-2}, with $\hat{\rho}$ slightly higher than $\delta\hat{W}_{\mathrm{core}}$. Since $|\delta\hat{W}_{\mathrm{fast}}| < \delta\hat{W}_{\mathrm{core}}$ and $\delta\hat{W}_{\mathrm{fast}} < 0$, we conclude that the criterion $-c_{\hat{\rho}}\hat{\rho}/\tau_{\mathrm{A}} < -\delta\hat{W}/\tau_{\mathrm{A}}$ in Eq. (3a) was satisfied. In these conditions, the sawtooth period is likely to have been determined principally by modifications in s_1, the magnetic shear at q = 1, and $s_{1,\mathrm{crit}}$ arising from the ion cyclotron current drive and electron heating, while the fast particle contribution $\delta\hat{W}_{\mathrm{fast}}$ does not play a role for triggering a sawtooth crash. This is confirmed by the consistency between the experimental and PRETOR-simulated sawtooth periods, when the effects due to fast particles are neglected in the PRETOR simulations.

As the resonance moves further inboard, a progressively higher portion of ICRF-accelerated ions have orbits lying entirely within the q = 1 surface and the fast ions become more energetic (since the power per ion increases as the effective deposition volume decreases). This results in an increase in the fast ion contribution to the n = 1, m = 1 internal kink mode energy $\delta\hat{W}_{\mathrm{fast}}$. As $\delta\hat{W}_{\mathrm{fast}}$ as given by Eq. (A.2) changes sign, due to a reversal in the fast ion diamagnetic direction, the fast ions become strongly stabilising. This appears to account for the observed gradual increase in the sawtooth period to about 230 ms as the resonance approaches gradually the magnetic axis. Thus, with the resonance well inside the q = 1 surface, sawtooth stabilisation by fast ion pressure [19] becomes important.

4.2 Effects of combined NBI and ICRF heating

4.2.1 Discharges with combined NBI and ICRF heating with the $\omega \approx 2\omega_{cH}$ resonance on the low field side

The results from Sections 4.1.1 and 4.1.2 indicate that control of sawteeth with a LFS $\omega \approx 2\omega_{\mathrm{cH}}$ resonance can be obtained by varying the resonance location rather than the ICRF phasing. Based on these results, experiments with a ramp in NBI power have been performed with $\omega \approx 2\omega_{\mathrm{cH}}$ resonance on the low field side at different magnetic fields to change the resonance position and thereby the sawtooth behaviour. They show that the normalised plasma beta at which NTMs are triggered can be increased in the presence of short-period sawteeth [3-5]. An overview of two representative discharges is shown in Fig. 10. In discharge 52083 with NBI and ICRF power tuned to a LFS resonance located outside the q = 1 surface (corresponding to the situation in discharge 51800 at $t \approx$ 22.8-23.2 s with a relatively short sawtooth period, cf. Fig. 2), sawteeth with a small amplitude and period were obtained. As the result, the normalised beta at the m = 3, n = 2 NTM onset was increased to $\beta_{\mathrm{N}} \approx 3.6$ as compared with similar discharge 52079 with the resonance close to the q = 1 surface (corresponding to the situation in discharge 51800 at $t \approx$ 24.5-24.9 s with a relatively long sawtooth period, cf. Fig. 2) and for which the $\beta_{\mathrm{N}} \approx 2.5$ at the NTM onset. Note that at the NTM onset at $t \approx$ 28 s in discharge 52083 the average coupled ICRF power has dropped to below 1 MW due to deteriorated ICRF coupling in the presence of edge localised modes (ELMs).

ICRF power partitioning and the total energy content of the ICRF-heated protons as given by the PION code for these discharges are shown in Fig. 11. As we can see by comparing Fig. 11 with ICRF power partitioning as shown in Fig. 3 for ICRF-only discharge 51800, the presence of the D beam ions does not change the power partitioning significantly for the LFS $\omega \approx 2\omega_{cH}$ resonance: hydrogen damping dominates both with and without deuterium NBI. Due to the somewhat larger coupled ICRF power, the proton energy content is larger for discharge 52083.

Figure 12 shows the results from the FIDO simulations for discharges 52083 and 52079 at $t \approx$ 23 s. As we can see, the main effect of the change in the magnetic field is, as expected, to change the radial location of the maximum current perturbation, collisional electron heating and fast ion pressure with respect to the sawtooth inversion radius located at $r/a \approx 0.25$.

4.2.2 Comparison of two discharges with and without deuterium NBI with the $\omega \approx 2\omega_{cH}$ resonance on the high field side

A comparison of two 1.2 T discharges with the same NBI power with and without ICRF, with the $\omega \approx 2\omega_{cH}$ resonance on the high field side, is shown in Fig 13. As we can see, the neutron rate is higher with ICRF at otherwise similar plasma conditions. Furthermore, the difference in the neutron rates with and without ICRF (up to NTM onset) correlates with the applied ICRF power. This suggests that the fusion reactivity could be enhanced due to parasitic deuteron absorption of the launched ICRF power. Indeed, the presence of deuterons with energies well above the critical energy [10] is confirmed by high-energy NPA measurements. Since no such neutron enhancement is observed with the $\omega \approx 2\omega_{cH} = 4\omega_{cD}$ resonance on the LFS in the presence of D beams, the most likely candidate is damping at the $\omega \approx 5\omega_{cD}$ resonance located in the plasma centre (i.e. between the $\omega \approx 2\omega_{cH}$ resonance and the low-field-side ICRF antennas, c.f. Fig. 1).

We have estimated, using the PION code, the level of parasitic deuteron absorption in the plasma centre consistent with the observed enhancement in the fusion reactivity. When ICRF power is set artificially to zero in the simulation, thus taking into account only the beam-thermal and thermal components to the fusion reactivity, the neutron rate as given by PION is

significantly smaller (by up to $\Delta R_{\mathrm{NT}} \approx 1.5\times10^{15}$ s^{-1}) than the measured neutron rate for discharge with ICRF in Fig 13. In order to explain the level and the time evolution of the measured neutron rate, we find that we need to assume that the deuteron absorption at the $\omega \approx 5\omega_{\mathrm{cD}}$ resonance increases from about 20% to about 30% of the applied ICRF power as the beam beta increases in time. Despite this weak parasitic deuteron damping, the NTM onset is clearly delayed in the discharge with combined ICRF and NBI as compared with the discharge with NBI only (cf. Fig 13). It should be noted that for discharge without ICRF in Fig 13 and other discharges considered in this article, the measured neutron rates are fully accounted for by the sum of thermal and beam-thermal fusion reactivities.

5. Conclusions and discussion

We have analysed ion cyclotron heating and current drive using ICRF waves tuned to the $\omega \approx 2\omega_{\mathrm{cH}}$ resonance in JET deuterium plasmas with a hydrogen concentration in the range of 5-15%. Differences in the plasma heating and current drive profiles have been studied at a fixed ICRF power of 4-5 MW for high field side (HFS) and low field side (LFS) resonances with waves propagating predominantly in either co-current or counter-current direction (+90° or –90° phasing, respectively). ICRF-only discharges have been considered with a ramp in the magnetic field and plasma current to change the resonance location at constant q to assess the effects on the sawtooth stability. Furthermore, discharges with combined ICRF and deuterium NBI have been analysed to study whether the added NBI power leads to new ICRF physics effects as the NBI injected deuterons are also resonant with the ICRF waves.

Our results indicate that second-harmonic hydrogen damping is maximized by placing the resonance on the LFS, which minimizes competing direct electron damping and parasitic high-harmonic D damping in the presence of D beams. The calculated current perturbation and electron heating profiles for the LFS resonance have been found to be consistent with the experimentally observed time behaviour of the sawtooth period when the resonance layer moves through the q=1 surface. The calculated driven current is dominated by a contribution of diamagnetic type caused by finite orbit widths of trapped resonating ions [7], giving rise to a decrease in the magnetic shear near the resonance, independent of the ICRF phasing. Note that the thin-banana-width approximation used in the Fisch model [6], taking into account

ICCD due to passing ions only, is not applicable in cases with a significant number of trapped ions, as pointed out earlier in Refs [7, 8]. Indeed, in cases with a strong trapped ion population a fast ion driven current given by the Fisch model can even be in the opposite direction than that given by detailed modelling with the 3D Monte Carlo code FIDO [13] used in Refs [7, 8] and in the present work. We have shown that placing the resonance on the HFS provides favorable conditions for the validity of the Fisch model as the ICRF-accelerated ion orbits become closer to the boundary between the passing and trapped orbits, hence increasing the number of passing ions.

Our results indicate that control of sawteeth with ion cyclotron current drive using the LFS $\omega \approx 2\omega_{cH}$ resonance in the present experimental conditions can be best obtained by varying the resonance location, while the ICRF phasing plays a negligible role. Based on these results, experiments with a ramp in NBI power have been performed at different magnetic fields, associated with resonance positions leading to different sawtooth periods. These experiments have shown that the normalised plasma beta at which $m = 3$, $n = 2$ neoclassical tearing modes (NTMs) are triggered can be increased in the presence of short-period sawteeth [3-5]. The effects due to the fast ion pressure on sawtooth stability have also been considered, and found to be stabilising when the resonance is well inside the $q = 1$ surface and small otherwise.

Due to differences in fast ion orbits for LFS and HFS resonances, collisional electron heating and fast ion pressure profiles are found to be significantly more peaked for a LFS resonance. The calculated differences in the fast ion populations, which we have illustrated by displaying a representative sample of fast ions in the orbit classification diagram outlined in Ref. 37, are supported by the fact that Alfvén eigenmodes driven by fast ions also have distinct characteristics in the LFS and HFS cases. For the HFS $\omega \approx 2\omega_{cH}$ resonance an additional ICRF physics effect has been observed. At low magnetic fields a careful comparison of discharges with and without ICRF power shows an enhanced neutron rate in the presence of D beam ions. This enhancement in fusion reactivity is found to be consistent with parasitic D damping of the applied ICRF power at the $\omega \approx 5\omega_{cD}$ resonance in the plasma centre (i.e. between the $\omega \approx 2\omega_{cH}$ resonance and the low-field-side ICRF antennas).

While sawtooth control with ICRF waves tuned to the $\omega \approx 2\omega_{cH}$ resonance has been demonstrated on JET to increase significantly the normalised plasma beta at which the $m = 3$,

n = 2 NTMs are triggered [3-5], its applicability to future reactor plasmas needs careful evaluation. For example, in ignited plasmas a hydrogen concentration in the range of 5-15%, as used in the present experiments, may be neither desirable nor practical, while for driven burn the plasma purity may be a less critical factor. However, the current drive mechanisms arising from finite-orbit-width effects and ICRF-induced transport of fast ions [7, 8] do not necessarily exclude operation at lower hydrogen concentrations than those used here. Another issue that is beyond the scope of our study and that would require a careful investigation when extrapolating the present scheme to reactor plasmas, is the possible parasitic absorption of the ICRF power by fusion born 3.5 MeV alpha particles. However, fewer complications exist for ICCD using the $\omega \approx 2\omega_{cT}$ scheme which is foreseen as the main ICRF scenario to be used in 50%:50% deuterium-tritium plasmas in next-step reactors. For this scenario the resonant ions are one of the fuel ion species and no alpha-particle resonances are located inside the plasma. Studies of second harmonic ICRF schemes in the present machines, such as $\omega \approx 2\omega_{cH}$ in JET discharges analysed in the present paper, are essential in order to predict with confidence the performance of ion cyclotron heating and current drive using the $\omega \approx 2\omega_{cT}$ scenario in a reactor.

Acknowledgement This work has been performed under the European Fusion Development Agreement. The work carried out by UKAEA personnel was partly funded by the UK Department of Trade and Industry, and EURATOM. The work carried out by C. Angioni and O. Sauter was partly funded by the Swiss National Science Foundation.

Appendix: Calculation of $\delta\hat{W}_{\mathrm{fast}}$

The contribution $\delta\hat{W}_{\mathrm{fast}}$ by ICRF-accelerated ions to the n = 1, m = 1 internal kink mode energy can be estimated approximately by assuming that essentially all the ICRF-accelerated ions inside q = 1 lie at $R \approx R_{\mathrm{res}}$. The fast particle contribution can then be approximated by the expression [41, 42]

$$\delta\hat{W}_{\mathrm{fast}} = -\frac{\pi^2}{\sqrt{6}s_1}\frac{\mu_0}{R_0 B_0}\left(\frac{R_0}{r_1}\right)^2 m_{\mathrm{h}} \int_0^{r_1} r\mathrm{d}r \int_{1/B_{\max}}^{1/B_{\min}} I_c(\lambda)\mathrm{d}\lambda \int_0^{\infty} \varepsilon^{3/2}\frac{\partial f}{\partial r}\mathrm{d}\varepsilon\,, \qquad \text{(A.1)}$$

where the subscript 1 refers to the q =1 surface, m_{h}, ε and f denote the mass, energy per unit mass and velocity distribution of the heated ions, respectively, and $I_c = \frac{1}{2\pi}\int_{-\theta_{\mathrm{b}}}^{\theta_{\mathrm{b}}} \frac{\cos\theta\,\mathrm{d}\theta}{\sqrt{1-\lambda B}}$, where θ_{b} is the poloidal angle of reflection. Here, we have taken into account a reduction in $\delta\hat{W}_{\mathrm{fast}}$ by approximately a factor of two arising from the fact that the most of the ICRF heated ions which cross the q = 1 surface have orbits that lie partly outside this surface [41].

By approximating the local ICRF-heated ion velocity distribution function by a bi-Maxwellian, strongly peaked at $r = r_1$, and using the approximation $I_c \approx \sqrt{R_0/2r}_1$ which is valid for small θ_{b} [42], we obtain from Eq. (A.1) the following estimate:

$$\delta\hat{W}_{\mathrm{fast}} \approx -\frac{\sqrt{3}\pi}{8}\frac{\mu_0 n_{\mathrm{h}} T_\perp}{B_0^2}\left(1+\frac{r_1 T_\perp}{R_0 T_\parallel}\right)^{-5/2}\sqrt{\frac{R_0}{2r_1}\frac{T_\perp}{T_\parallel}}\left(\frac{r_1 - r_{\mathrm{res}}}{r_1 s_1}\right), \qquad \text{(A.2)}$$

where $T_\perp$, $T_\parallel$ and n_{h} are the perpendicular temperature, parallel temperature and density of ICRF-heated ions, respectively. The negative sign in this equation arises from the fact that the fast ion pressure gradient is assumed to rise as r approaches r_1, giving a reversal in the usual direction of the fast ion diamagnetic drift.

In order to estimate $\delta\hat{W}_{\mathrm{fast}}$ in more detail, analysis with sophisticated kinetic-magnetohydrodynamic codes such as CASTOR-K [43] would be required. Such analysis is beyond the scope of the present article and left for a further study.

References

[1] D.F.H. Start, *et al*., in Proceedings of the International Conference on Plasma Physics, Innsbruck, 1992 (European Physical Society, Geneva, 1992), Vol. 16C, Part II, p. 897.

[2] V.P. Bhatnagar, *et al*., Nucl. Fusion 34 1579 (1994).

[3] O. Sauter, *et al*., 'Neoclassical Tearing Mode Seed Island Control with ICRH in JET', in Proceedings of 28th EPS Conference on Controlled Fusion and Plasma Physics, Funchal, Madeira, 2001 (European Physical Society, Geneva, 2001), in press.

[4] M.-L. Mayoral, *et al*., 'Sawtooth and Neoclassical Tearing Mode Seed Island Control by ICRF Current drive on JET', in Radio Frequency Power in Plasmas (14th Topical Conference, Oxnard, California 2001), AIP Conference Proceedings 595, American Institute of Physics, New York (2001), p. 106.

[5] E. Westerhof, *et al.*, 'Control of neoclassical tearing modes by sawtooth control with ion cyclotron resonance frequency waves in JET', to be submitted to Nucl. Fusion (2001).

[6] N.J. Fisch, Nucl. Fusion 21, 15 (1981).

[7] T. Hellsten, J. Carlsson, L-G Eriksson, Phys. Rev. Letters 74, 3612 (1995).

[8] J. Carlsson, T. Hellsten, J. Hedin, Phys. Plasmas 5, 2885 (1998).

[9] F. Nguyen, *et al*., ICRF Current Drive Experiments on JET,' to be submitted to Plasma Phys. Control. Fusion; F. Nguyen, *et al*., ICRF Current Drive Experiments on JET,' in Proceedings of 28th EPS Conference on Controlled Fusion and Plasma Physics, Funchal, Madeira, 2001 (European Physical Society, Geneva, 2001), in press.

[10] T.H. Stix, Plasma Physics 14, 367 (1972).

[11] L.-G. Eriksson, T. Hellsten and U. Willén, Nucl. Fusion 33, 1037 (1993).

[12] L.-G. Eriksson and T. Hellsten, Phys. Scripta 55, 70 (1995).

[13] J. Carlsson, L.-G. Eriksson and T. Hellsten, in Theory of Fusion Plasmas (Proc. Joint Varenna-Lausanne Int. Workshop, Varenna, 1994), Editrice Compositori, Bologna (1994) 351.

[14] D. Boucher and P.H. Rebut, in Proc. IAEA Tech. Com. on Advanced in Simulation and Modelling of Thermonuclear Plasmas, 1992, Montreal (1993), p. 142.

[15] F. Porcelli, D. Boucher and M.N. Rosenbluth, Plasma Phys. Control. Fusion 38, 2163 (1996).

[16] D. J. Campbell, *et al*., Phys. Rev. Lett. 60, 2148 (1988).

[17] C.K. Phillips, *et al.*, Phys. Fluids B4, 2155 (1992).

[18] M. Zabiego, *et al*., Proceedings of the 15th International Conference on Plasma Physics and Controlled Nuclear Fusion Research, IAEA, Seville, 1994, Plasma Physics and Controlled Nuclear Fusion Research, IAEA-CN-60/D-18, Vol. **3**, 399 (IAEA, Vienna, 1996).

[19] F. Porcelli, Plasma Phys. Control. Fusion 33,1601 (1991).

[20] C. Angioni, *et al*., in Theory Fusion Plasmas (Proc. Joint Varenna-Lausanne Int. Workshop, Varenna, 2000), Editrice Compositori, Bologna (2000) 73.

[21] M.A. Henderson, *et al*., Fusion Eng. Design 53, 241 (2001).

[22] O. Sauter, *et al*., Phys. Plasmas 8, 2199 (2001).

[23] O. Sauter, *et al.*, in Theory of Fusion Plasmas, Proc. Joint Varenna-Lausanne Int. Workshop, Varenna, 1998, Editrice Compositori, Bologna (1999) 403.

[24] T. Hellsten and L. Villard, Nucl. Fusion 28, 285 (1988).

[25] T. Hellsten and L.-G. Eriksson, Nucl. Fusion 29, 2165 (1989).

[26] X. Llobet, T. Hellsten, L. Villard, in Theory of Fusion Plasmas (Proc. Varenna Lausanne Int. Workshop Chexbres, 1988), Editrice Compositori, Bologna (1988) p. 663.

[27] M.J. Mantsinen, *et al.*, Plasma Phys. Control. Fusion 41, 843 (1999).

[28] L.-G. Eriksson and P. Helander, Phys. Plasmas 1, 308 (1994).

[29] L. Chen, J. Vaclavik, and G. Hammett, Nucl. Fusion 28, 389 (1988).

[30] J. Hedin, *et al*., Plasma Phys. Control. Fusion 40, 1085 (1998).

[31] A. Fasoli, *et al*., Plasma Phys. Control. Fusion 39, Suppl. 12B, B287 (1997).

[32] R. Heeter, *et al*., in Proceedings of the 5th IAEA Technical Committee Meeting on Alpha Particles in Fusion Research, 8-11 September, 1997, JET, United Kingdom.

[33] T. Ohkawa, Nuclear Fusion 10, 185 (1970).

[34] J.W. Connor and J.G. Cordey, Nucl. Fusion 14, 185 (1974).

[35] D.F.H. Start, J.G. Cordey, and E.M. Jones, Plasma Phys. 22, 303 (1980).

[36] S.C. Chiu, *et al*., Nucl. Fusion 23, 499 (1983).

[37] L.-G. Eriksson and F. Porcelli, Plasma Phys. Control. Fusion 43, R145 (2001).

[38] W. Kerner, *et al*., Nucl. Fusion 38, 1315 (1998).

[39] A.A. Korotkov, A. Gondhalekar, and A.J. Stuart, Nucl. Fusion 37, 35 (1997).

[40] P.H. Rebut, P.P. Lallia, M.L. Watkins, Plasma Phys. Control. Fusion 11, 172 (1987).

[41] P. Helander, P. Lisak, Plasma Phys. 47, 281 (1992).

[42] R.O. Dendy, *et al*., Phys. Plasmas 2, 1623 (1995).

[43] D. Borba and W. Kerner, Journ. Comput. Phys. 153, 101 (1999).

Table 1 Discharges analysed in this article. In all discharges ICRF power was applied at a frequency of 42 MHz. The magnetic axis is at $R \approx 3$ m.

Pulse	P_{ICRF}/P_{NBI} (MW)	B_0 (T)	I_p (MA)	R (m) at $\omega \approx 2\omega_{cH}$	n_H/n_D (%)	ICRF phasing
51800	4.5 / blips	1.6→1.4	1.6→1.2	3.6→2.9	12.5	-90°
51801	4.5 / blips	1.6→1.4	1.6→1.2	3.6→2.9	12.5	+90°
51796	4.7 / blips	1.0→1.4	1.0→1.4	2.2→3.0	9	-90°
52079	3.8 / 2.4→14	1.5	1.5	3.2	10-13	-90°
52083	4.5 / 2.4→17	1.6	1.55	3.4	10-14	-90°
51994	4.6 / 2.1→15.3	1.2	1.2	2.5	5-7	-90°

Figures

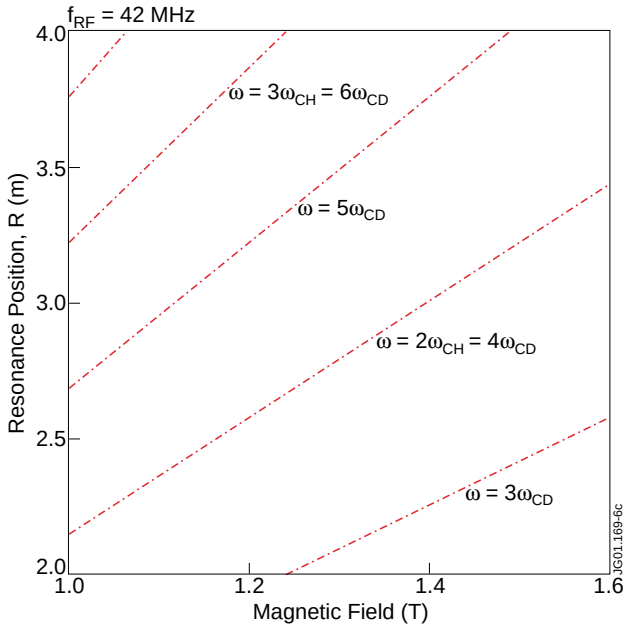

Figure 1 Ion cyclotron resonance locations for protons and deuterons as a function of the toroidal magnetic field for an ICRF frequency of 42 MHz. Here, we have assumed $B = B_0 R_0 / R$ and R_0 = 3 m. The minor radius of a JET plasma is about 1 m.

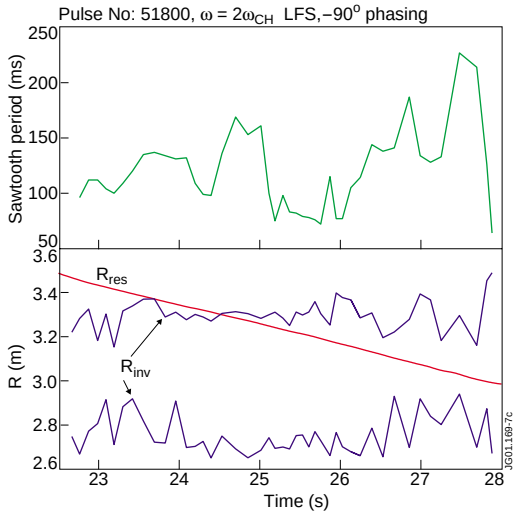

Figure 2 Sawtooth period and the $\omega \approx 2\omega_{\mathrm{H}}$ resonance and inversion radius locations for discharge 51800**.** The magnetic axis is at $R \approx 3$ m.

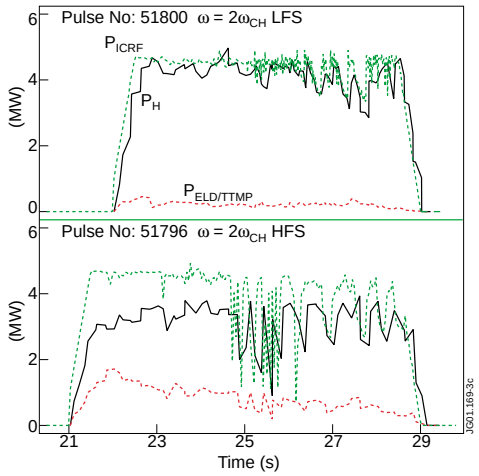

Figure 3 Power partitioning as given by PION for discharges 51800 and 51796, respectively.

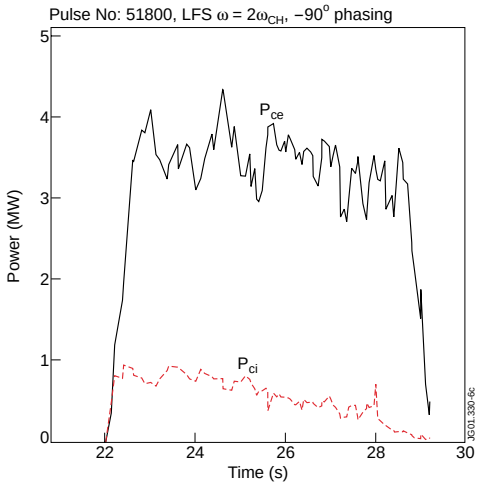

Figure 4 Collisional electron and ion heating as given by PION for discharge 51800.

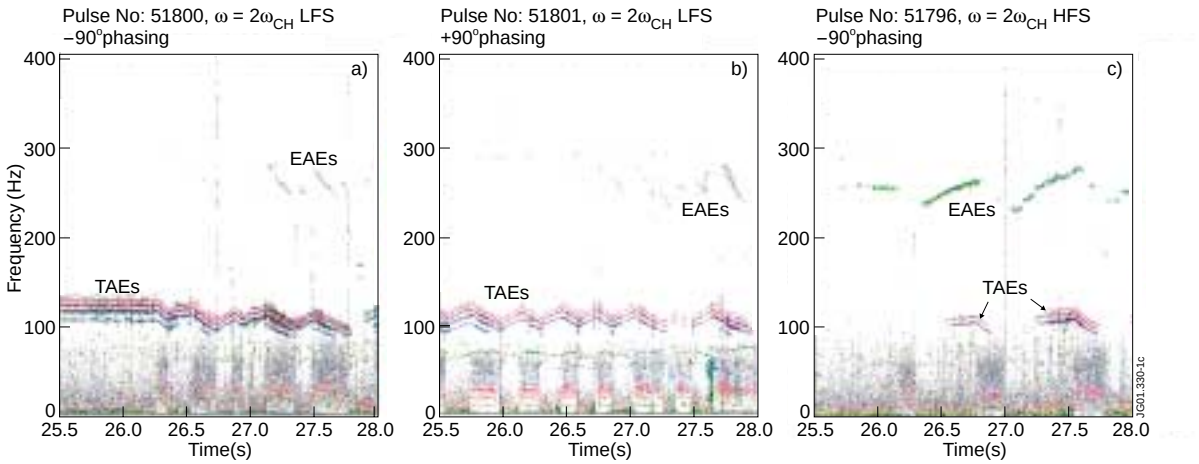

Figure 5 Magnetic fluctuation spectrograms measured with the magnetic pick-up coils at the plasma edge in discharges 51800, 51801 and 51796.

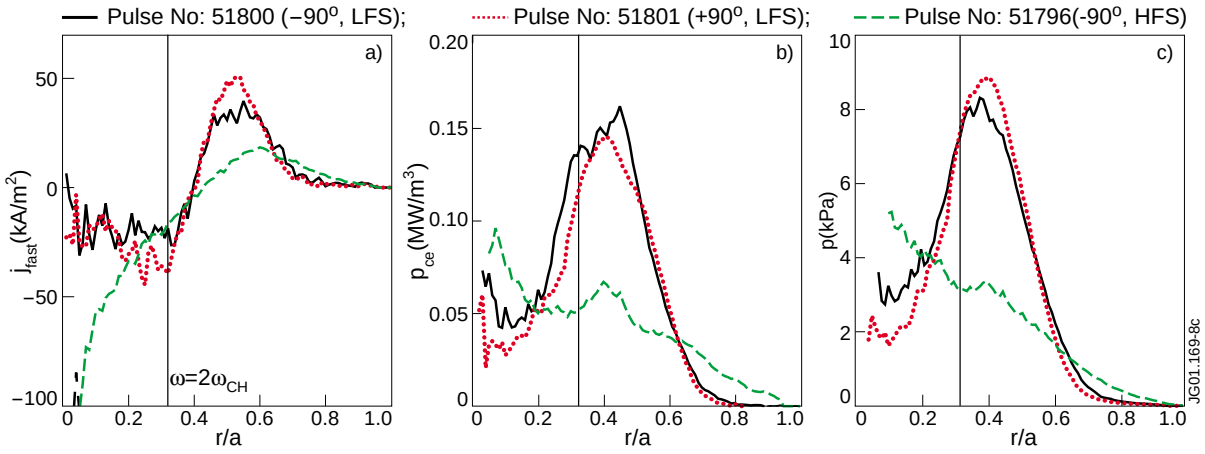

Figure 6 (a) Current density driven by ICRF-accelerated protons, (b) collisional electron heating power density and (c) fast proton pressure profile as given by FIDO for discharges 51800, 51801 and 51796. Here, the $\omega \approx 2\omega_{cH}$ resonance is at $r/a = 0.32$ in all cases.

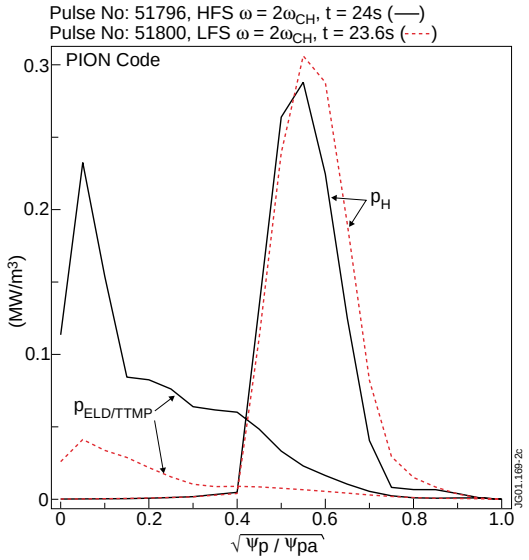

Figure 7 Calculated direct electron and H absorption profiles as given by PION for discharges 51800 and 51796 with a LFS and HFS resonance, respectively.

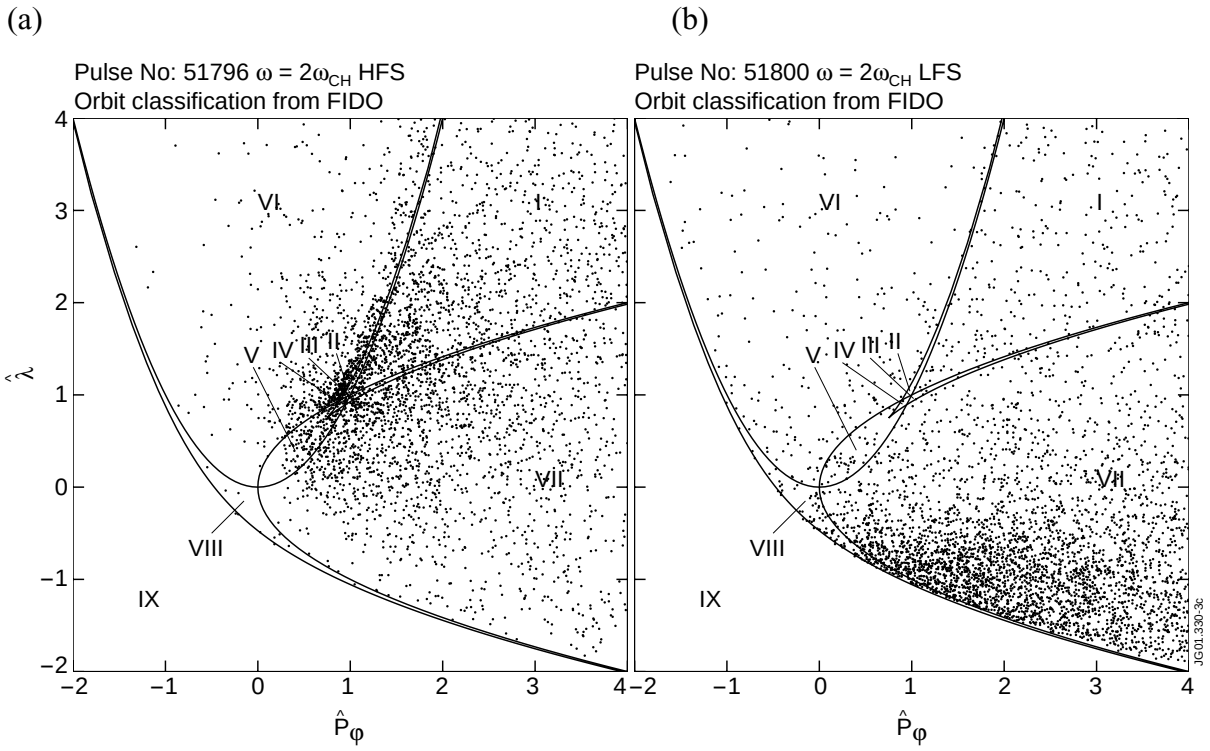

Figure 8 Orbit classification diagrams showing results from FIDO simulations for (a) discharge 51796 and (b) discharge 51800 with a HFS and LFS $\omega \approx 2\omega_{cH}$ resonance, respectively. The different regions of this diagram are defined and extensively discussed in Ref. 37.

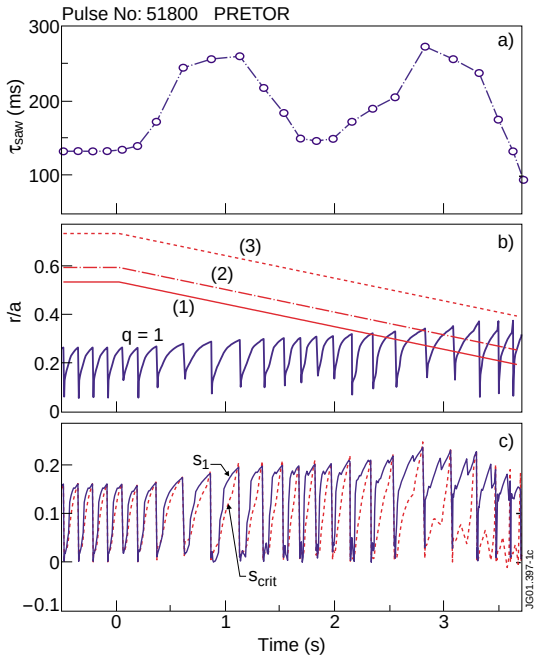

Figure 9 (a) Sawtooth period given by PRETOR for discharge 51800, assuming the time evolution of the maxima of (1) the counter current drive density, (2) the heating power density and (3) the co current drive density as shown in (b) together with the simulated $q = 1$ radius. The radial profiles of the current and heating power densities are assumed to be Gaussians with profile widths fitting the FIDO results. The shear and the critical shear at $q = 1$, which are relevant for the sawtooth trigger criterion given by Eq. (3b), are displayed in (c). Here, the times $t = 0$ and 3.5 s correspond to $t \approx 22.5$ and 26 s, respectively, in Fig. 2.

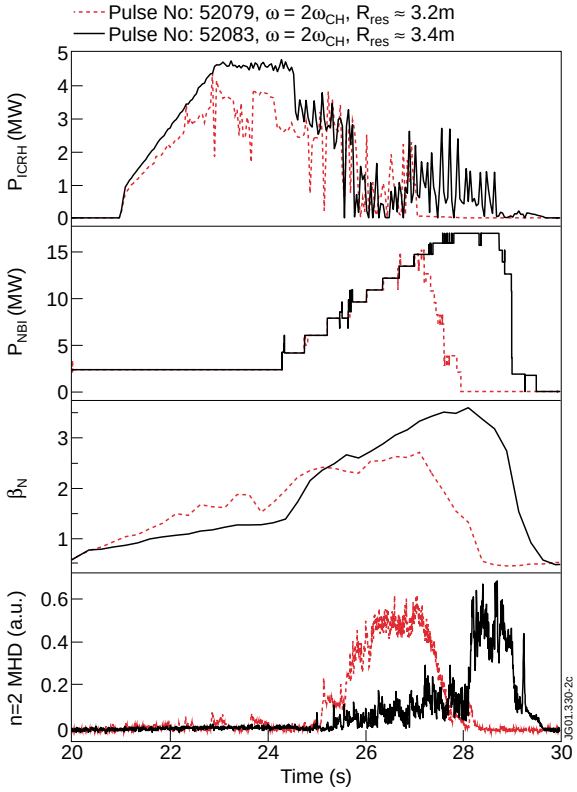

Figure 10 Overview of discharges 52079 and 52083 with ICRF power tuned to a LFS $\omega \approx 2\omega_{cH}$ resonance at $R_{res} \approx 3.2$ m and 3.4 m, respectively.

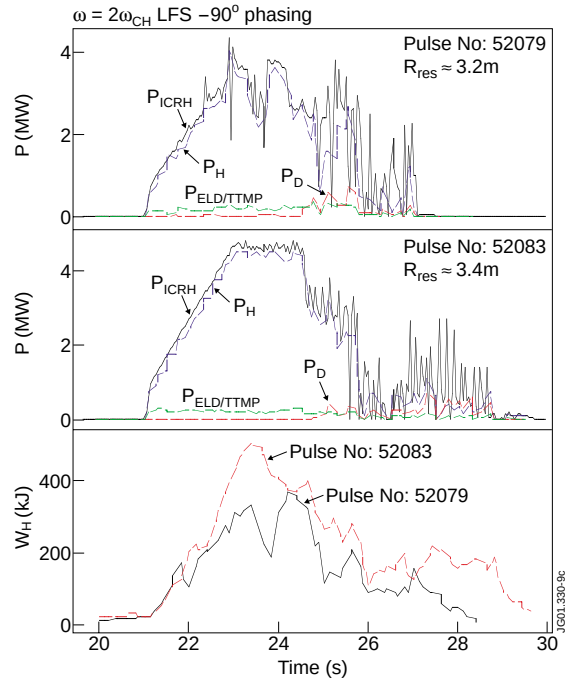

Figure 11 ICRF power partitioning as given by PION (a) for discharge 52079 with $R_{res} \approx 3.2$ m and (b) for discharge 52083 with $R_{res} \approx 3.4$ m. In (c) the energy content of hydrogen ions as given by PION are also shown for these two discharges.

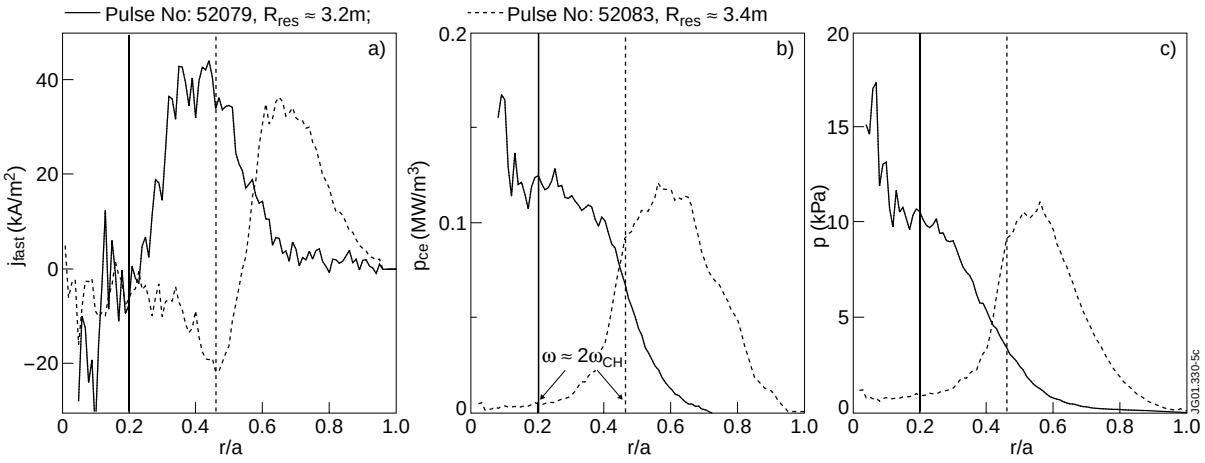

Figure 12 (a) Current density driven by ICRF-accelerated protons, (b) collisional electron heating power density and (c) fast proton pressure profile as given by FIDO for discharges 52079 (solid) and 52083 (dotted). The corresponding $\omega \approx 2\omega_{cH}$ resonance locations are also shown. The sawtooth inversion radius is located at $r/a \approx 0.25$ in both discharges.

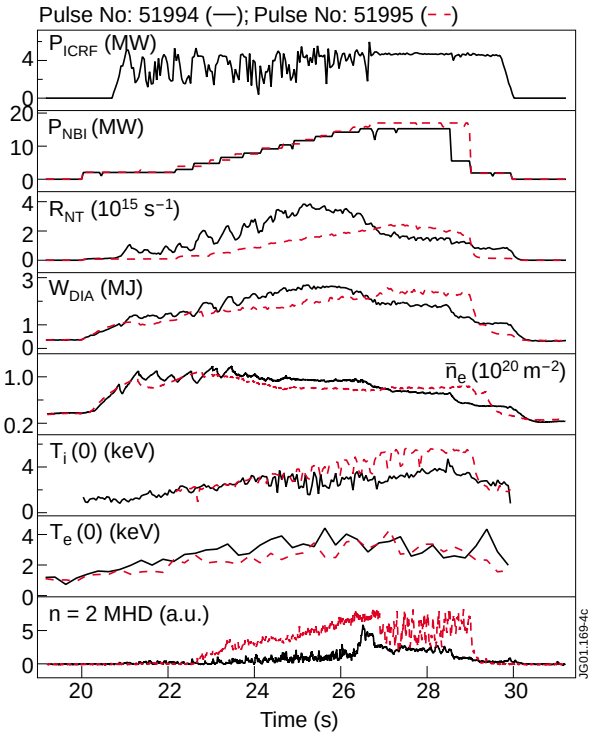

Figure 13 Overview of discharges 51994 and 51995 with and without ICRF power tuned to a HFS $\omega \approx 2\omega_{cH}$ resonance.